

X-ray absorption lines in the Seyfert 1 galaxy NGC 5548 discovered with Chandra-LETGS

J.S. Kaastra¹, R. Mewe¹, D.A. Liedahl², S. Komossa³, and A.C. Brinkman¹

¹ SRON Laboratory for Space Research Sorbonnelaan 2, 3584 CA Utrecht, The Netherlands

² Physics Department, Lawrence Livermore National Laboratory, P.O. Box 808, L-11, Livermore, CA 94550, USA

³ Max Planck Institut für Extraterrestrische Physik, Postfach 1603, D-85740 Garching, Germany

Received 1-Feb-2000 / Accepted 4-Feb-2000

Abstract. We present for the first time a high-resolution X-ray spectrum of a Seyfert galaxy. The Chandra-LETGS spectrum of NGC 5548 shows strong, narrow absorption lines from highly ionised species (the H-like and He-like ions of C, N, O, Ne, Na, Mg, Si, as well as Fe XIV – Fe XXI). The lines are blueshifted by a few hundred km/s. The corresponding continuum absorption edges are weak or absent. The absorbing medium can be modelled by an outflowing, thin and warm shell in photoionization equilibrium. The absorption lines are similar to lower ionization absorption lines observed in the UV, although these UV lines originate from a different location or phase of the absorbing medium. Redshifted with respect to the absorption lines, emission from the O VIII Ly α line as well as the O VII triplet is visible. The flux of these lines is consistent with emission from the absorbing medium. The O VII triplet intensity ratios demonstrate that photoionization dominates and yield an upper limit to the electron density of $7 \times 10^{16} \text{ m}^{-3}$.

Key words: Galaxies: individual: NGC 5548 – Galaxies: Seyfert – quasars: absorption lines – – X-rays: galaxies

1. Introduction

Low to medium energy resolution X-ray spectra of AGN such as obtained by the Rosat or ASCA observatories showed the presence of warm absorbing material (see references in Kaastra 1999). This was deduced from broad band fits to the continuum, showing a flux deficit at wavelengths shorter than the expected edges of ions such as O VII and O VIII. The relation of this warm X-ray absorber to the medium that produces narrow UV absorption lines in C IV or N V is not clear, mainly due to a lack of sufficient constraints in the X-ray band. A major drawback of all previous X-ray studies of AGN has been the low spectral resolution, making it hard to disentangle any emission line features from the surrounding absorption edges, and prohibiting the measurements of Doppler shifts or broadening. With the Chandra spectrometers it is now possible for the first time to obtain high-resolution X-ray spectra of AGN.

Send offprint requests to: J.S. Kaastra
Correspondence to: J.Kaastra@sron.nl

2. Observations

The present Chandra observations were obtained on December 11/12, 1999, with an effective exposure time of 86400 s. The detector used was the High Resolution Camera (HRC-S) in combination with the Low Energy Transmission Grating (LETG). The spectral resolution of the instrument is about 0.06 Å and almost constant over the entire wavelength range (1.5–180 Å). Event selection and background subtraction were done using the same standard processing as used for the first-light observation of Capella (Brinkman et al. 2000). The wavelength scale is currently known to be accurate to within 15 mÅ. The efficiency calibration has not yet been finished, and our efficiency estimates are based upon preflight estimates for wavelengths below 60 Å and on inflight calibration based upon data from Sirius B for longer wavelengths. We estimate that the current effective area is accurate to about 20–30 %, that it may show large scale systematic variations within those limits, but it does not show significant small scale variations.

The observed count spectrum was corrected for higher spectral order contamination by subtracting at longer wavelengths the properly scaled observed count spectrum at shorter wavelengths. The spectrum was then converted to flux units by dividing it by the effective area, and by correcting for the galactic absorption of $1.65 \times 10^{24} \text{ m}^{-2}$ (Nandra et al. 1993), as well as for the cosmological redshift, for which we took the value of 0.01676 (Crenshaw et al. 1999). The spectrum in the 5–38 Å range is shown in Fig. 1. The continuum is rather smooth; the reality of the large-scale structures cannot be assessed completely at this moment given our current understanding of the efficiency calibration of the instrument. Nevertheless, there is no indication for the presence of strong O VII or O VIII K-shell absorption edges at 16.77 and 14.23 Å, respectively. A more detailed discussion of the spectrum, including the long-wavelength part will be given in a forthcoming paper, when the full efficiency calibration of the instrument is available.

2.1. Absorption lines

The most striking feature of the spectrum is the presence of narrow absorption lines, including the Lyman α and β transitions

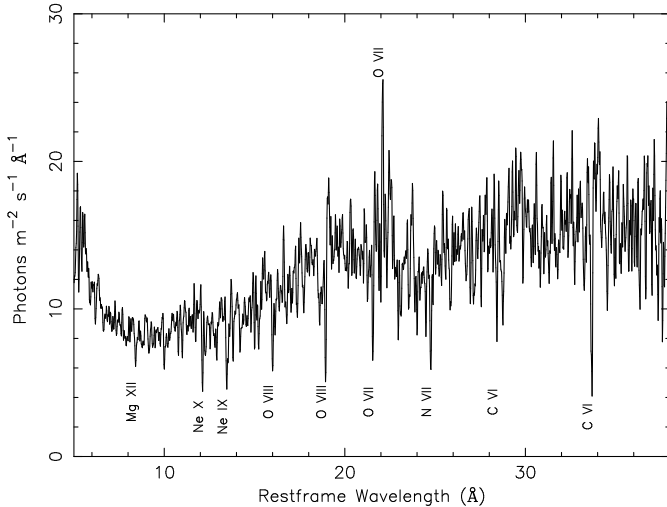


Fig. 1. Chandra LETGS X-ray spectrum of NGC 5548, corrected for order contamination, redshift and galactic absorption.

of H-like C, N, O, Ne and Mg, as well as the 2–1 resonance absorption line of He-like O and Ne. We have searched the wavelength range of Fig. 1 systematically for absorption and emission lines, and found the lines listed in Table 1. In addition we provide data for some weaker features for which the equivalent widths (or their upper limits) help to constrain models. We give expected wavelength λ_0 , the measured wavelength difference $\Delta\lambda \equiv \lambda_0 - \lambda_{obs}/(1+z)$ (thereby accounting for the cosmological redshift z), the equivalent line width W (determined from a gaussian fit to the line profile), and the proposed line identification. A negative sign before an equivalent width indicates an emission line. The presence of these absorption lines can be seen as evidence for a warm, absorbing medium in NGC 5548 along the line of sight towards the nucleus. The absorption can be very strong: the core of the C VI Ly α line for example absorbs some 90 % of the continuum, and this is just a lower limit, since the true line profile is smeared out by the instrument. That the optical depth in some lines is considerable is evidenced by two facts: firstly, the equivalent width ratio of the Ly β to Ly α lines of C VI and O VIII is much larger than the ratio of their oscillator strengths (0.079 to 0.417). Secondly, we see absorption features of sodium, despite the fact that the sodium abundance is 20 times smaller than, e.g., the magnesium abundance. All this can be explained if the line cores of the more abundant elements are strongly saturated.

2.2. Column densities

Using the observed equivalent width W of the absorption lines, it is possible to derive the absorbing column density, assuming a gaussian velocity distribution (standard deviation σ_v) of the

Table 1. Absorption and emission lines identified in NGC 5548. Lines possibly blended by lines from other ions are indicated by an asterisk.

λ_0 (Å)	$\Delta\lambda$ (mÅ)	W (mÅ)	Identification
5.217	57 ± 25	19 ± 15	Si XIV 1s - 3p (Ly β)
6.182	12 ± 16	18 ± 7	Si XIV 1s - 2p (Ly α)
8.421	1 ± 11	24 ± 8	Mg XII 1s - 2p (Ly α)
9.169	-9 ± 29	14 ± 9	Mg XI 1s ² - 1s2p ¹ P ₁ (r)
9.314	-19 ± 0	-9 ± 11	Mg XI 1s ² - 1s2s ³ S ₁ (f)
10.025	-16 ± 15	21 ± 10	Na XI 1s - 2p (Ly α)
11.003	8 ± 13	21 ± 10	Na X 1s ² - 1s2p ¹ P ₁ (r)
12.134	0 ± 7	38 ± 9	Ne X 1s - 2p (Ly α) *
12.274	13 ± 21	26 ± 9	Fe XVII 2p-4d *
12.292	-5 ± 21	26 ± 9	Fe XXI 2p-3d *
12.844	-27 ± 23	16 ± 11	Fe XX 2p-3d blend
12.904	-4 ± 12	25 ± 11	Fe XX 2p-3d
13.447	21 ± 8	46 ± 9	Ne IX 1s ² - 1s2p ¹ P ₁ (r) *
13.522	26 ± 12	25 ± 11	Fe XIX 2p-3d blend
13.698	24 ± 32	-18 ± 13	Ne IX 1s ² - 1s2s ³ S ₁ (f)
13.826	59 ± 11	26 ± 10	Fe XVII 2p-3p
14.207	0 ± 14	22 ± 10	Fe XVIII 2p-3d blend
15.014	5 ± 12	19 ± 10	Fe XVII 2p-3d
15.176	64 ± 13	25 ± 9	O VIII 1s - 4p (Ly γ)
15.265	-39 ± 13	25 ± 9	Fe XVII 2p-3d
16.006	7 ± 10	40 ± 9	O VIII 1s - 3p (Ly β)
16.612	10 ± 11	-45 ± 15	No id
17.396	-19 ± 28	20 ± 10	O VII 1s ² - 1s5p ¹ P ₁
17.768	-25 ± 17	22 ± 10	O VII 1s ² - 1s4p ¹ P ₁
18.627	-7 ± 17	21 ± 10	O VII 1s ² - 1s3p ¹ P ₁
18.969	-22 ± 7	55 ± 10	O VIII 1s - 2p (Ly α)
21.602	-40 ± 10	53 ± 12	O VII 1s ² - 1s2p ¹ P ₁ (r)
21.602	70 ± 15	-33 ± 16	O VII 1s ² - 1s2p ¹ P ₁ (r)
21.804	25 ± 17	-33 ± 19	O VII 1s ² - 1s2p ³ P _{1,2} (i)
22.101	11 ± 11	-64 ± 19	O VII 1s ² - 1s2s ³ S ₁ (f)
24.781	-4 ± 12	54 ± 14	N VII 1s - 2p (Ly α)
28.466	-25 ± 11	36 ± 12	C VI 1s - 3p (Ly β)
33.736	-36 ± 10	99 ± 17	C VI 1s - 2p (Ly α)
38.950	-88 ± 25	35 ± 22	Fe XV 3s ² -3s5p
39.146	25 ± 25	164 ± 61	No id
40.268	-46 ± 45	216 ± 82	C V 1s ² - 1s2p ¹ P ₁ (r)
50.350	-11 ± 32	47 ± 30	Fe XVI 3s-4p
52.911	-36 ± 12	73 ± 21	Fe XV 3s ² -3s4p
58.963	-9 ± 52	48 ± 40	Fe XIV 3p-4d

absorbing ions and neglecting the scattered line emission contribution:

$$W = \frac{\lambda\sigma_v}{c} \int_{-\infty}^{\infty} [1 - \exp(-\tau_0 e^{-y^2/2})] dy, \quad (1)$$

with τ_0 the optical depth of the line at the line center, given by

$$\tau_0 = 0.106 f N_{20} \lambda / \sigma_{v,100}. \quad (2)$$

Here f is the oscillator strength, λ the wavelength in Å, $\sigma_{v,100}$ the velocity dispersion in units of 100 km/s and N_{20} the column density of the ion in units of 10^{20} m^{-2} . Given a value for σ_v and the measured equivalent width, these equations yield the

column density. For some ions we have more than one absorption line identified, and this allows us to constrain σ_v . From the O VII, O VIII and C VI ions we obtain $\sigma_v=140\pm30$ km/s. Using this value, we derive the column densities of Table 2. We

Table 2. Derived column densities

ion	$\log N$ observed (m^{-2})	$\log N$ model (m^{-2})	ion	$\log N$ observed (m^{-2})	$\log N$ model (m^{-2})
C VI	21.2 ± 0.3	21.2	Si XIV	22.6 ± 1.6	19.8
N VII	21.1 ± 0.5	21.0	Fe XIV	19.9 ± 0.7	20.1
O VII	21.2 ± 0.3	21.3	Fe XV	20.3 ± 0.2	20.1
O VIII	22.1 ± 0.3	22.1	Fe XVI	20.4 ± 0.5	19.6
Ne IX	$<22.8\pm1.2$	21.1	Fe XVII	20.5 ± 0.3	20.5
Ne X	$<22.6\pm1.1$	21.2	Fe XVIII	20.3 ± 0.5	20.4
Na X	20.9 ± 0.8	-	Fe XIX	20.6 ± 0.7	20.0
Na XI	21.4 ± 1.0	-	Fe XX	20.9 ± 0.5	19.3
Mg XI	20.8 ± 0.7	20.8	Fe XXI	$<20.9\pm0.7$	18.2
Mg XII	22.3 ± 1.3	20.4			

give the column density N in logarithmic units. The reason is the relatively large inferred optical depth of some lines, e.g. 70 for the O VIII Ly α line. This makes the line core saturated and hence significant changes in the column density lead to minor changes in the equivalent width.

One of the most striking features of the spectrum is the absence of the oxygen continuum absorption edges that were deduced from low resolution X-ray spectra such as those acquired with Rosat (Nandra et al. 1993), ASCA (Fabian et al. 1994) or BeppoSAX (Nicastro et al. 2000). The absence is, however, consistent with the column densities derived above from the line absorption. We predict a jump of 11 % at the O VIII edge (14.23 Å) and 4 % at the O VII edge (16.77 Å), all within a factor of 2. We can measure any jumps near the edges with an accuracy of about 10 % of the continuum, but we find no evidence for an absorption edge; the data even suggest a small emission edge (radiative recombination continuum) of 10 ± 10 %.

The column densities of the other ions for which we have absorption measurements do not lead to significant absorption edges, except for Ne IX and Ne X, which should be at the low side of their column density range in order to avoid significant continuum absorption. Note that the Ne X Ly α line has some blending from Fe XVII 4d-2p; taking that into account leads to a somewhat smaller column density.

We have made a set of runs using the XSTAR photoionization code (Kallman & Krolik 1999), using solar abundances and the spectral shape as given by Mathur et al. (1995), normalised to 13 photons $\text{m}^{-2}\text{s}^{-1}\text{\AA}^{-1}$ at 20 Å. We obtained a good overall agreement with our measured column densities using a hydrogen column density of $3\times10^{25}\text{ m}^{-2}$ and $\xi=100\pm25$ (in units of 10^{-9} W m). This column density is comparable to the value derived from earlier ASCA observations (Fabian et al. 1994). However, our ionization parameter is significantly larger, having most of the oxygen as O VIII or O IX. The plasma temperature of the absorber implied by the

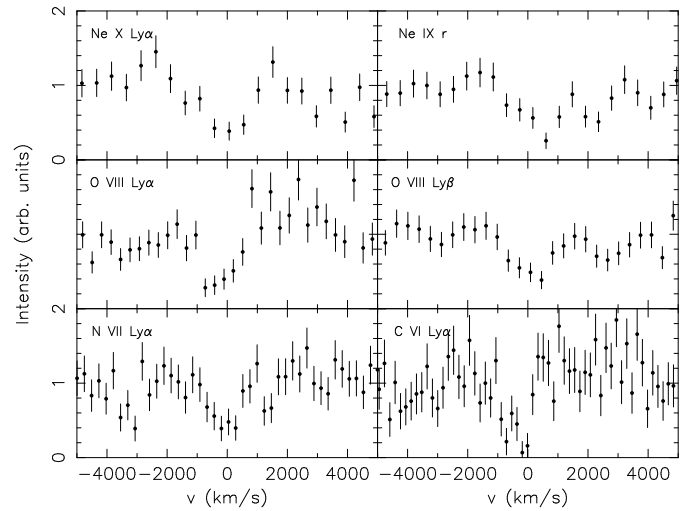


Fig. 2. Line profile for six absorption lines. The intensity is scaled to 1 in the $\pm(5000-10000)$ km/s range. Bin size is 0.02 Å.

XSTAR model is 2×10^5 K. The low temperatures imply that thermal contributions to line broadening (σ_v) are negligible.

2.3. Velocity fields

The absorption lines appear to be blueshifted: the average blueshift of the C, N and O lines is 280 ± 70 km/s. There is some evidence that the lines are broadened in proportion to their wavelengths, indicative of Doppler broadening. Subtracting the instrumental line width ($\sigma=0.023$ Å) yields for the intrinsic line broadening a width (σ) of 270 ± 100 km/s, somewhat larger than the width of 140 km/s derived from line ratios (previous section). This could indicate that the absorber consists of a few narrow components ($\sigma\sim140$ km/s), with different mean velocities and $\sigma\sim270$ km/s for the ensemble. As an illustration we show the velocity profile of six of the strongest absorption lines in Fig. 2. On the blue side, the line profiles extend out to about 2000 km/s. There is no clear evidence for the presence of an underlying broad emission component for these lines, although for O VIII and C VI there appears to be an excess at the red side of the absorption line.

2.4. Emission lines

The LETGS spectrum of NGC 5548 shows only a few emission lines. Except for a clear detection of the He-like triplet of O VII, we only identified the forbidden lines of the same triplets of Ne IX and Mg XI; these are marginally detected. Here we focus upon the O VII triplet (Fig. 3). The forbidden (f) and intercombination (i) line are not blue-shifted like the absorption lines but have a marginally significant redshift of 200 ± 130 km/s. The ratio i/f can be used as a density diagnostic if the coupling between the upper levels (2^3S and 2^3P) of f and i is determined by electron collisions and not by the external radiation field from the central source. For a photon flux of 50 pho-

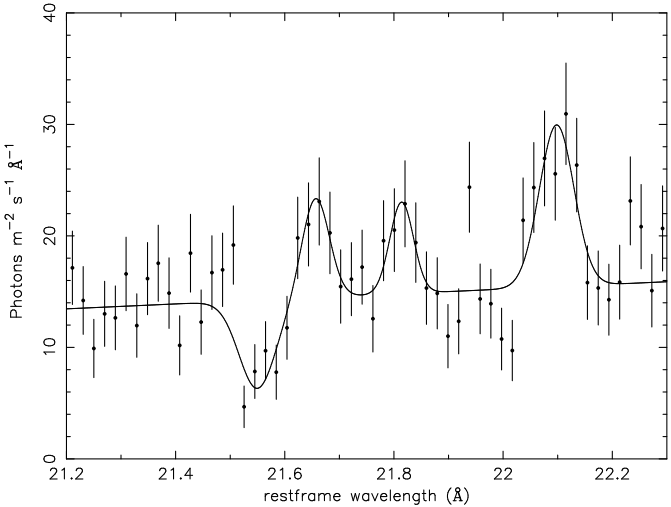


Fig. 3. Spectrum near the O VII triplet (data with error bars) plus a simple model fit (continuum plus gaussian lines) for the main absorption and emission components discussed in the text.

tons $\text{m}^{-2}\text{s}^{-1}\text{Å}^{-1}$ at 1600 Å and the atomic parameters taken from Porquet & Dubau (2000) we estimate that this is the case as long as $n_e > 4 \times 10^{14} \text{ m}^{-3}$. The ratio i/f does depend only weakly upon the type of ionization balance: Collisional ionization equilibrium (CIE) or photoionization equilibrium (PIE) (Mewe 1999 and Porquet & Dubau 2000). From the observed value i/f of 0.45 ± 0.29 we derive an upper limit to the electron density n_e of $7 \times 10^{16} \text{ m}^{-3}$. The observed ratio $G = (i+f)/r$ is 3.2 ± 1.5 , although this value might be somewhat smaller due to overlap of the r absorption component. For CIE plasmas, G should be of order 1, while for PIE plasmas, values larger than about 4 can be expected (Liedahl 1999, Porquet & Dubau 2000). Thus, the O VII triplet probably originates from a photoionized plasma. Does the emission from the triplet arise from the same medium that absorbs the continuum? Assuming that the absorber has the shape of a thin, spherical shell, we calculate on the basis of recombination and the absorber parameters derived in section 2.2 emission line intensities that agree within the error bars with the measured intensities. The upper limit for n_e found from the i/f ratio then implies a lower limit for the thickness of the shell of $5 \times 10^8 \text{ m}$, and a distance from the central source of at least $8 \times 10^{13} \text{ m}$. Thus, both the absorption and emission of the O VII resonance line, as well as the emission from i and f may originate in the same expanding shell.

3. Discussion

For the first time we see narrow absorption lines in the X-ray spectrum of an AGN. However narrow absorption lines in Seyfert galaxies have been seen before in the UV band. Shull and Sachs (1993) discovered narrow absorption features in the C IV and N V lines. This was confirmed by Mathur et al. (1995) and studied in more detail by Mathur et al. (1999) and Crenshaw et al. (1999). These last authors find at least 5 narrow ab-

sorption components in the C IV 1550 Å and N V 1240 Å lines. These components are broadened by $\sigma_v = 20\text{--}80 \text{ km/s}$, somewhat smaller than we find. The rms width of the ensemble of UV absorption lines is 160 km/s for C IV and 260 km/s for N V, consistent with the effective line width of $270 \pm 100 \text{ km/s}$ that we find from our Chandra data. Also, the average blueshift of the UV absorption lines (-390 km/s for C IV and -490 km/s for N V) is only slightly larger than what we find for the C, N and O lines ($-280 \pm 70 \text{ km/s}$). Note that our wavelength scale has residual uncertainties of 100–300 km/s for most of our lines.

However, the column density of the lithium-like ions C IV and N V as derived by Crenshaw et al. is 100 times smaller than the column density of the corresponding hydrogen-like ions that we find. The difference may be attributed to either time variability (low column density during the UV observations), a high degree of ionization (hydrogenic ions dominating) or a stratified absorber (with UV and X-ray absorption lines originating from different zones). We favour this last possibility. This is supported by the fact that our simulations with XSTAR imply C IV and N V columns that are 100 times smaller than the measured values by Crenshaw et al.

Crenshaw & Kraemer (1999) find that the weakest of the five dynamical components (their number 1) in the UV absorption lines has the highest outflow velocity (-1056 km/s). Based upon the N V to C IV ratio, they argue that this component has the highest ionization parameter and could produce the oxygen continuum absorption edges as implied by the ASCA data. Our modelling with XSTAR also predicts column densities of N V and C IV close to the measured values for component 1. But the outflow velocity of the X-ray absorber that we find is significantly smaller than the velocity of UV component 1. However, Mathur et al. (1999) identify component 3 (-540 km/s) as the most likely counterpart to the X-ray warm absorber. We conclude that the detailed relation between UV and X-ray absorbers is still an open issue.

Acknowledgements. The Laboratory for Space Research Utrecht is supported financially by NWO, the Netherlands Organization for Scientific Research. Work at LLNL was performed under the auspices of the U.S. Department of Energy, Contract No. W-7405-Eng-48.

References

- Brinkman, A.C., Gunsing, C.J.T., Kaastra, J.S., et al., 2000, ApJ 530, L111
- Crenshaw, D.M., Kraemer, S.B., Boggess, A., et al., 1999, ApJ 516, 750
- Crenshaw, D.M., Kraemer, S.B., 1999, ApJ 521, 572
- Fabian, A.C., Nandra, K., Brandt, W.N., et al., 1994, in: *New Horizons of X-ray Astronomy*, p. 573, eds. Makino, F. & Ohashi, T., Univ. Ac. Press.
- Kaastra, J.S., 1999, in: *X-ray spectroscopy in astrophysics*, p. 269, eds. van Paradijs, J. & Bleeker, J.A.M., Springer.
- Kallman, T.R., Krolik, J.H., 1999, XSTAR photoionization code, ftp://legacy.gsfc.nasa.gov/software/plasma_codes/xstar/
- Liedahl, D.A., 1999, in: *X-ray spectroscopy in astrophysics*, p. 189, eds. van Paradijs, J. & Bleeker, J.A.M., Springer.

Mathur, S., Elvis, M., Wilkes, B., 1995, *ApJ* 452, 230
Mathur, S., Elvis, M., Wilkes, B., 1999, *ApJ* 519, 605
Mewe, R., 1999, in: X-ray spectroscopy in astrophysics, p. 109, eds.
van Paradijs, J. & Bleeker, J.A.M., Springer.
Nandra, K., Fabian, A.C., George, I.M., et al., 1993, *MNRAS* 260,
504
Nicastro, F., de Rosa, A., Feroci, M., et al., 2000, *ApJ*, in press
Porquet, D., Dubau, J., 2000, *A&A*, in press
Shull, J.M., Sachs, E.R., 1993, *ApJ* 416, 536